Dual-Strategy Optimization of Reference Systems Enhances Reliability in Tumor DNA Methylation Detection: Primer-Probe Innovation for Low-Concentration Clinical Specimens

Shan Zhang [1,#] , Jiahui Jiang [2,#], Ling Chen [3,*]

[1.] 427000 Zhangjiajie, Department of Gynecology, Zhangjiajie People's Hospital

[2.] 450046 Zhengzhou, College of Life Sciences, Henan Agricultural University

[3.] 430030 Wuhan, Tongji Hospital, Tongji Medical College, Huazhong University of Science and Technology

[#] Equal contribution

[*] Corresponding author

Ling Chen

Tongji Hospital, Tongji Medical College, Huazhong University of Science and Technology, Wuhan, China. E-mail: lingchen@hust.edu.cn

ABSTRACT

DNA methylation biomarkers are crucial for early cancer detection, yet quantitative methylation-specific PCR (qMSP) faces significant challenges with low-concentration clinical samples due to suboptimal reference systems, leading to inadequate sample classification and wasted specimens. To address this, we developed optimized reference primer-probe sets through a dual-phase strategy: first, optimizing published bisulfite-converted ACTB (bisACTB) primers and designing novel CpG-free bisACTB primers, validated via SYBR Green qPCR using bisHela templates; second, coupling top-performing primers with probes for rigorous TaqMan qPCR evaluation across diverse biospecimens (cell lines, gender-matched tissues, plasma/serum). Results identified two optimized bisACTB_103 primer-probe sets exhibiting significantly enhanced sensitivity and specificity in probe-based qPCR, alongside novel high-performing candidates including the CpG-free bisProAB1_F2+R2+P1 set. Comparative analysis revealed bisACTB_103_F2+R2+P2 and bisProAB1_F2+R2+P1 as the top performers overall, demonstrating significantly improved amplification efficiency ($p<0.01$)

across all sample types, with pronounced gains in low-concentration plasma (ΔCt = -1.5, 2.8-fold sensitivity increase). This study establishes two robust reference systems that enhance detection pass rates for challenging low-input samples and provide standardized ΔCt-based quality metrics for reliable qMSP assay validation in clinical diagnostics applications.

KEYWORDS

DNA methylation biomarkers, Quantitative methylation-specific PCR (qMSP), Reference system optimization, ACTB, Cell-free DNA (cfDNA), Low-concentration plasma detection, ΔCt-based quality metric, Early cancer detection.

INTRODUCTION

DNA methylation biomarkers hold significant value for the early screening and diagnosis of human cancers[1-3]。Quantitative methylation-specific PCR (qMSP) is a widely used technique for detecting these biomarkers, primarily employing two detection chemistries: the dye-based method (SYBR Green) and the probe-based method (hydrolysis probe, e.g., TaqMan)[4]. This technique targets bisulfite-converted DNA (bisDNA), the modified sequence derived from human genomic DNA (gDNA) after sodium bisulfite treatment. Currently, commercially available DNA methylation detection kits predominantly utilize probe-based qPCR. qMSP has been extensively applied to detect various malignancies, including colorectal cancer[5,6], head and neck cancer[7], lung cancer[8], liver cancer[9,10], breast cancer[11,12], gynecological cancers[13,14], and urothelial carcinoma[15,16]. The biospecimens analyzed encompass diverse clinical sample types such as stool[17], saliva[7,18], bronchoalveolar lavage fluid (BALF)[19], tissue[20,21], cervical exfoliated cells[14], urine[15,16], and blood (plasma/serum)[21-25]. In the aforementioned studies, the Cycle threshold (Ct) value range from the reference gene channel in qMSP assays is commonly used as a criterion to assess both DNA yield and sample adequacy. Similarly, commercial kits define sample acceptability based on a predetermined reasonable Ct range for the reference channel in probe-based qPCR. However, existing reference primer-probe sets frequently suffer from suboptimal amplification efficiency, resulting in elevated Ct values. This can lead to the misclassification of adequate samples as inadequate, causing wastage of valuable clinical

specimens. Furthermore, the performance of reference primer-probe combinations reported in the literature and used in commercial kits is highly variable. Critically, there is a notable lack of systematic studies dedicated to optimizing and comparatively evaluating reference systems for qMSP.

This study addresses these limitations through a dual-strategy approach. First, focusing on the commonly used *ACTB* reference gene primer-probe combinations in studies involving colorectal cancer stool samples, esophageal cancer blood/plasma samples, and liver/colorectal cancer blood samples, we performed sequence optimization. This yielded enhanced primer-probe sets demonstrating superior amplification efficiency (targeting bisACTB) and heightened specificity (minimizing amplification of unconverted gACTB). Second, we conducted a comprehensive analysis of the human ACTB gene and its 2000 bp upstream promoter region. Three CpG-free sequences were identified as candidate target regions. Novel reference primer-probe sets were designed based on the bisulfite-converted sense strand sequences of these regions, with several exhibiting excellent bisACTB amplification performance. The findings provide substantial dual benefits to the research and clinical communities. First, we deliver high-performance qMSP reference candidate sets, enabling significant improvements in the detection pass rate for low-concentration clinical samples. Second, the established optimized and novel reference systems provide a unified standard for performance comparison across different reagents, facilitating the standardization of detection methodologies.

MATERIALS AND METHODS

Human Specimens

All samples (tissue and blood) were residual material obtained following the completion of routine clinical diagnostic procedures. Specifically, the paired cancer tissues and adjacent normal tissues consisted of archived frozen remnants from standard pathological examinations, while the preoperative peripheral blood samples, obtained from patients with benign gynecological conditions or malignancies, were residual aliquots collected in EDTA-K2 anticoagulant tubes for standard clinical testing; these samples were sourced specifically from the Department of Gynecology at Zhangjiajie People's

Hospital.

Cells, Reagents, and Instruments

The HeLa, HT29, and 293T cell lines were purchased from Procell Life Science & Technology Co., Ltd (Wuhan, China; Cat# CL-0101, CL-0118, CL-0005). SYBR Green I qPCR Master Mix (Cat# TSE501) was obtained from Tsingke Biotechnology Co., Ltd (Wuhan, China). Hot-start Taq DNA polymerase for probe-based qPCR (Cat# HMD0206-01) was provided by HaiGene Biotech Co., Ltd. Primers and probes were synthesized by Sangon Biotech (Shanghai, China) and Biologics Co., Ltd (Shanghai, China), with high-performance liquid chromatography (HPLC) purification. Key instruments and kits included a real-time PCR system (SLAN-96S; Hongshi Medical Technology, Shanghai), along with DNA extraction kits - specifically column-based genomic DNA extraction kits for cells/tissues (DP304-03; Tiangen Biotech, Beijing) and magnetic bead-based plasma DNA extraction kits (N902-02; Novizan Biotechnology, Nanjing). For bisulfite conversion, we utilized both column-based (Cat# 122-002; GeneTech, Shanghai) and magnetic bead-based (EM103-01; Novizan Biotechnology, Nanjing) purification kits. Finally, DNA quantification was performed using a NanoDrop™ One spectrophotometer (840-317400; Thermo Fisher Scientific).

Primers and Probes Design

All primers were designed using Primer Premier 5 software with melting temperatures (Tm) of 58–62□. Probes were designed with Primer Express 3.0.1, featuring 5′-VIC fluorophore and 3′-MGB quencher modifications (Tm: 68–73□).

NCBI Primer-BLAST Analysis

Primer specificity was evaluated using NCBI Primer-BLAST (https://www.ncbi.nlm.nih.gov/tools/primer-blast/), where forward and reverse primers were entered in their respective fields. The analysis was performed using the "Genomes for selected eukaryotic organisms (primary assembly only)" database with Homo sapiens specified as the target organism, while maintaining default settings for the "Get Primers" function. The output results provided comprehensive information including genomic specificity profiles and

amplicon size distributions.

DNA Extraction and Bisulfite Conversion

Genomic DNA from cell lines, blood cells, and tissues was extracted using Tiangen column-based kits. For bisulfite conversion, 2 μg gDNA (≤30 μL) was processed with GeneTech's column-based kit, followed by bisDNA quantification (NanoDrop™ One). Plasma DNA was extracted using Novizan's magnetic bead-based kit, with 30 μL converted using their bead-based bisulfite kit. All steps followed manufacturers' protocols.

SYBR Green qPCR

Primer performance assessment was conducted using three controls: (1) negative control consisting of gDNA from HeLa cells (1 ng/μL), (2) positive control containing bisDNA from HeLa cells (0.5 ng/μL), and (3) no-template control with ddH□O. All qPCR reactions were performed in triplicate using a 20 μL reaction mixture comprising 10 μL of 2× SYBR Green I master mix, 0.4 μL each of forward and reverse primers (10 μM), and 2 μL of template DNA. The thermal cycling protocol consisted of an initial denaturation at 95°C for 1 min, followed by 45 cycles of denaturation at 95°C for 15 s and annealing/extension at 60°C for 15 s (with fluorescence acquisition at this stage). Subsequently, melting curve analysis was performed by gradually increasing the temperature from 60°C to 95°C at a rate of 0.03°C per second while continuously monitoring fluorescence.

Probe-Based qPCR

Validation of primer-probe combinations was performed using negative and positive controls as described above. The qPCR reactions were carried out in a final volume of 25 μL containing 0.1 μL of Hot-start Taq DNA polymerase, 2.5 μL of 10× reaction Buffer, 0.25 μL each of forward and reverse primers and probe (10 μM), and 2 μL of template DNA. The thermal cycling conditions consisted of an initial incubation at 25°C for 10 min, followed by denaturation at 95°C for 2 min, and 50 cycles of amplification (95°C for 15 s and 60°C for 20 s, with fluorescence acquisition during the 60°C step). For sample testing, we used either 0.5 ng/μL of bisulfite-converted DNA (for cells, tissues, and blood cells) or 2 μL of undiluted plasma-derived bisDNA, with all reactions

performed in triplicate.

Data Visualization

All figures were generated using GraphPad Prism 8.0.2. For SYBR Green assays, melting/amplification curves were exported from PCR instruments and plotted with uniform axis scales. Probe-based qPCR amplification curves were processed similarly. Images were exported as 300-dpi TIFF files.

Statistical Analysis

Intergroup comparisons used two-tailed Student's *t*-tests, with statistical significance set at $P < 0.05$.

Results

Rational Optimization of *ACTB* Primer Sets Enhances Bisulfite-Specific Amplification Fidelity in qMSP Assays

Housekeeping genes, such as *ACTB*, are commonly used as internal reference controls in qMSP for tumor studies. Based on primer sequences targeting the region gACTB_103 (containing 2 CpG sites; see Supplementary Sequence Information) reported by Zhang et al.[26], Wang et al. [27], and Bian et al.[28,29], we designated this primer pair as bisACTB_103_F1 (F1: AAGGTGGTTGGGTGGTTGTTTTG) and bisACTB_103_R1 (R1: AATAACACCCCCACCCTGC), though sequence analysis revealed an A-to-G mutation at the second base from the 3' end in R1 (Supplementary Sequence Information). To address potential limitations, we optimized the primers: Firstly, F1 was shortened by 2 nucleotides to bisACTB_103_F2 (F2: GTGGTTGGGTGGTTGTTTTG), reducing Tm from 64.8°C to 58.3°C. Secondly, R1 was extended by 4 nucleotides (avoiding the 3' mutation) to bisACTB_103_R2 (R2: TTTTAATAACACCCCCACCCTAC), maintaining Tm near 59.5°C. Additionally, mutant bisACTB_103_F2_17C (F2_17C: GTGCTTGGGTGGTTGTTTTG) was designed to reduce dimerization with R2. Incomplete bisulfite conversion (<100% efficiency) results in residual gDNA, which acts as a potent source of non-specific amplification in qMSP. Consequently, SYBR Green I-based qPCR was utilized to simultaneously assess three key parameters: (i) amplification efficiency of the bisACTB target, quantified using Ct values; (ii) product specificity evaluated through melting

curve analysis for both bisDNA and gDNA templates; and (iii) primer-dimer artifact formation in no-template controls (NTCs). For this purpose, gDNA extracted from HeLa cells (gHeLa) and its bisulfite-converted counterpart (bisHeLa) served as template sources, while nuclease-free water functioned as the blank control (BC). Results demonstrated that F1+R1 amplified BC (Ct=33.55, melt peak 75-80°C; Fig. 1A), indicating primer dimers. Although specific amplification was observed for both gHeLa (Ct=25.62; Tm=85-90°C) and bisHeLa (Ct=29.67; Tm=80-85°C; Fig. 1A,D; Table 1), the substantially lower Ct value for gHeLa indicated significant contamination risk from unconverted DNA. In contrast, optimized pair F2+R2 produced only primer-dimer peaks when amplifying gHeLa (Fig. 1B), while exhibiting markedly reduced Ct values for bisHeLa (25.82 vs. 29.67; $p<0.01$, Fig. 1D,E; Table 1), demonstrating elimination of gDNA amplification and enhanced bisACTB targeting efficiency. Furthermore, F2_17C+R2 displayed negligible dimer formation (undetectable in BC, Fig. 1C), absence of gDNA amplification products, and superior bisHeLa amplification efficiency (Ct=27.72; Fig. 1D,F; Table 1). Computational validation via NCBI Primer-BLAST identified a 103-bp genomic target for F1+R1, whereas no homologous targets were predicted for optimized primer sets (Supplementary Sequence Information), corroborating experimental findings. Collectively, these results establish that both optimized primer pairs (F2+R2 and F2_17C+R2) effectively mitigate gDNA interference and improve bisACTB amplification, with F2_17C+R2 exhibiting minimal dimerization and thus representing an optimal internal reference for SYBR Green I-based qMSP in DNA methylation studies.

Subsequent optimization targeted the *ACTB* primer pair reported by Li et al. [30]and Zhao et al. [31], which amplifies a bisACTB_89 fragment (89 bp; GC content 38-40%; containing 2 CpG sites, Supplementary Sequence Information). The original primers were designated as bisACTB_89_FP (FP: CGCAATAAATCTAAACAAACTCC), bisACTB_89_RP-1 (RP-1: GGGTTAGATGGGGGATATGT), and bisACTB_89_RP-2 (RP-2: AGGTTAGACGGGGGATATGT). To enhance thermodynamic properties, FP was extended by one nucleotide to generate bisACTB_89_R (R: CCGCAATAAATCTAAACAAACTCC), increasing its Tm from 56.4°C to 59.8°C, while RP-1/RP-2 were extended by five nucleotides to create bisACTB_89_F

(F: CAGTTAGGTTAGATGGGGGATATGT), elevating Tm from 55.2°C/57.9°C to 60.2°C. Comparative qPCR analysis revealed that the original primer combinations (FP+RP-1 and FP+RP-2) exhibited inefficient bisHeLa amplification (Ct = 33.32 and 32.39, respectively; Fig. 2D,E; Table 3) despite showing no detectable amplification with gHeLa or blank controls (Fig. 2A,B,D,E). Conversely, the optimized F+R pair demonstrated significantly improved amplification efficiency for bisHeLa (Ct = 29.11; Fig. 2F; Table 3) without generating non-specific products (Fig. 2C,F). Although NCBI Primer-BLAST analysis indicated no predicted genomic amplicons for either primer set, the optimized F+R pair provides substantially enhanced bisACTB amplification efficacy, establishing its utility as a robust internal reference for qMSP assays.

Finally, we optimized the *ACTB* primer pair reported by Wang et al. [32], targeting a bisACTB_78 fragment (78 bp; GC content 37-38%; containing 1 CpG site, Supplementary Sequence Information). The original primers, designated bisACTB_78_F2 (F2: GGGATATGTAGAAAGTGTAAAG) and bisACTB_78_R2 (R2: CACAATAAATCTAAACAAACTCC), were modified as follows: F2 was extended by three nucleotides to generate bisACTB_78_F3 (F3: TGGGGGATATGTAGAAAGTGTAAAG; Tm increased from 48.7°C to 59.2°C) and its mutant derivative bisACTB_78_F3_19C (F3_19C: GGGGGCTATGTAGAAAGTGTAAAG; Tm 59.8°C), while R2 was substituted with the previously optimized bisACTB_89_R (Tm increased from 51.6°C to 59.8°C). qPCR evaluation demonstrated that the original F2+R2 combination exhibited inefficient bisHeLa amplification (Ct = 38.55; Fig. 3D; Table 5), whereas the optimized F3_19C+R pair achieved significantly enhanced amplification efficiency (Ct = 30.32; Fig. 3F; Table 5) without detectable amplification in gHeLa or blank controls (Fig. 3C,F). Critically, F3_19C+R produced a single melting curve peak for bisHeLa (Tm 75-80°C; Fig. 3C), consistent with expected product characteristics. Bioinformatic analysis indicated three low-significance genomic targets for F2+R2 via NCBI Primer-BLAST, while no comparable targets were predicted for optimized primers. Consequently, F3_19C+R demonstrates high-specificity bisACTB amplification with undetectable gDNA interference and negligible dimer formation, establishing it as a high-fidelity internal reference for SYBR Green

I-based qMSP in DNA methylation studies.

Rational Probe Engineering Enhances TaqMan Assay Fidelity for bisACTB Methylation Detection

Minor groove binder (MGB)-modified probes are widely employed in TaqMan probe-based qPCR for DNA methylation analysis due to their high specificity, shorter sequence requirements, and low fluorescent background[33-35]. Accordingly, all TaqMan qPCR assays in this study utilized MGB probes. However, since the probe sequence (GGAGTGGTTTTTGGGTTTG) used by Zhang et al.[26], Wang et al.[27], and Bian et al.[28,29] initiates with a guanine (G) at its 5'-end—a suboptimal configuration for MGB probes—we redesigned a universal probe sequence designated bisACTB_103_P2 (abbreviated P2: AAACCTCCAAACAACC). This modification avoids a 5'-terminal G while positioning the probe closer to the 3'-end of the reverse primer than in published designs, thereby theoretically enhancing 5' nuclease cleavage efficiency by Taq polymerase and improving signal-to-noise ratios. TaqMan qPCR results demonstrated that optimized primer-probe sets F2+R2+P2 and F2_17C+R2+P2 achieved significantly lower Ct values for bisHeLa amplification (28.33 and 28.54, respectively) compared to F1+R1+P2 (30.35) (Fig. 1A; Supplementary Table 2). Critically, no amplification was observed for gHeLa with either optimized set, whereas F1+R1+P2 showed partial amplification in replicates (Fig. 1B; Supplementary Table 2). All sets exhibited no amplification in blank controls (BC) (Fig. 1C; Supplementary Table 2). Collectively, these results confirm enhanced bisACTB targeting efficiency and absence of gDNA interference with optimized primer-probe combinations.

For the ACTB primer sets from Li et al.[30]and Zhao et al.[31], which shared the probe sequence TCCCAAAACCCCAACACAC, we designated a universal probe bisACTB_89_P (abbreviated P). TaqMan qPCR analysis revealed no significant difference in bisHeLa amplification efficiency between original (FP+RP-1+P and FP+RP-2+P) and optimized (F+R+P) primer-probe sets (Fig. 1D; Supplementary Table 4). Moreover, no amplification occurred with gHeLa or BC templates, indicating equivalent performance between literature-derived and optimized configurations in TaqMan assays.

Regarding the probe sequence (CCCAACACACTTAACCA) used by Wang et al.[32]with *ACTB* primers—designated bisACTB_78_P2 (P2)—its distal

positioning relative to the 3'-end of bisACTB_78_R2 theoretically reduces Taq polymerase exonuclease activity, yielding suboptimal signal-to-noise ratios. To address this, we substituted P2 with bisACTB_89_P (P), which resides closer to the reverse primer's 3'-end, and paired it with optimized primers F3+R and F3_19C+R. Notably, the original F2+R2+P2 set exhibited low plateau signal intensity, poor signal-to-noise ratio, and non-canonical amplification curves for bisHeLa (Fig. 1G). In contrast, optimized sets F3+R+P and F3_19C+R+P displayed significantly higher plateau signals and signal-to-noise ratios with canonical sigmoidal curves (Fig. 1G), validating that proximity between the probe's 5'-end and primer's 3'-end enhances detection sensitivity. While Ct values showed no significant differences across sets (Fig. 1G; Supplementary Table 6), confirming comparable amplification kinetics, all sets demonstrated equivalent specificity with no amplification in gHeLa or BC samples (Fig. 1H,I). Collectively, we established two optimized internal reference systems: (i) bisACTB_103_F2 + bisACTB_103_R2 + bisACTB_103_P2, which demonstrated significantly enhanced amplification efficiency compared to literature-reported configurations; (ii) bisACTB_78_F3 + bisACTB_89_R + bisACTB_89_P, which exhibited substantially improved amplification kinetics and signal-to-noise ratios. Both systems serve as robust internal references for TaqMan probe-based qPCR in tumor DNA methylation studies.

CpG-Free Reference Systems Enable Robust DNA Methylation Quantification

Since the gACTB fragments (gACTB_103, ACTB_89, and ACTB_78) referenced in prior studies contain ≥1 CpG site (Supplementary Sequence Information), bisulfite conversion may introduce T/C heterogeneity at these positions, resulting in sequence non-uniqueness (Supplementary Sequence Information). This variability could impair sample identification reliability when amplifying internal reference targets. To circumvent this limitation, we selected two CpG-free gACTB sequences and one *ACTB* promoter fragment[36], designated gAB1, gAB2, and gProAB1 (Supplementary Sequence Information). Their bisulfite-converted counterparts (bisAB1, bisAB2, bisProAB1) exhibit sequence uniqueness, for which we designed dedicated primers and probes (Supplementary Table 14). NCBI Primer-BLAST analysis confirmed no predicted human genomic targets of comparable size for these novel primer sets (data not shown).

SYBR Green I qPCR revealed broad or multi-peak melting curves for bisAB1/bisAB2 primer sets during bisHeLa amplification (data not shown); conversely, three bisProAB1 primer sets—F+R[36] (133 bp; 33% GC), F1+R1 (64 bp; 38% GC), and F2+R2 (78 bp; 35% GC)—generated single, sharp melting peaks for bisHeLa (Tm 75-80°C; Fig. 4A), consistent with predicted characteristics. Although Ct values showed no significant differences between F+R and F1+R1/F2+R2 (Fig. 4D; Supplementary Table 7), all sets exhibited primer dimers or non-specific amplification with gHeLa (Fig. 4B,E), and critically, only F+R lacked dimer peaks in blank controls (Fig. 4C,F). Thus, these reference sets are unsuitable for SYBR Green I-based tumor DNA methylation studies.

Given these limitations, TaqMan qPCR was employed to identify optimal configurations: For bisAB1, F4+R4+P4 demonstrated the lowest Ct (29.56) with canonical sigmoidal curves (Fig. 2A,D,G) and no gHeLa/BC amplification (Fig. 2B,C,E,F,H,I; Supplementary Table 8); for bisAB2, F4+R4+P4 showed suboptimal kinetics (non-sigmoidal curve, Ct=29.81; Fig. 2J) despite no gHeLa/BC amplification (Fig. 2K,L; Supplementary Table 8); whereas for bisProAB1, F2+R2+P1 achieved the minimal Ct (28.74; Fig. 3A; Supplementary Table 9) among tested combinations with undetectable background interference (Fig. 3B,C; Supplementary Table 9). Consequently, experimental validation established F4+R4+P4 (bisAB1), F4+R4+P4 (bisAB2), and F2+R2+P1 (bisProAB1) as optimal primer-probe sets.

In summary, through systematic screening of novel primers and probes targeting CpG-free bisACTB sequences derived from gACTB fragments, we established validated optimal primer-probe sets for two bisACTB segments and one bisProACTB segment.

Optimized Primer-Probe Systems Demonstrate Superior Efficiency and Kinetics in Cell-Based Methylation Analysis

To comprehensively evaluate optimized primer-probe configurations, we defined comparative groups: Control Group 1 (original bisACTB_103_F1+R1+P2) versus Optimized Group 1 (bisACTB_103_F2+R2+P2); Control Groups 2-1/2-2 (bisACTB_89_FP+RP-1/P and FP+RP-2/P) versus Optimized Group 2 (bisACTB_89_F+R+P); Control Group 3 (bisACTB_78_F2+R2+P2) versus Optimized Group 3

(bisACTB_78_F3+bisACTB_89_R+P); and Control Group 4 (bisProAB1_F+R+P) versus Optimized Groups 4-1/4-2/4-3 (bisProAB1_F2+R2+P1, bisAB1_F4+R4+P4, bisAB2_F4+R4+P4). Subsequently, TaqMan qPCR was performed using bisDNA from human renal (293T) and colorectal carcinoma (HT29) cell lines. Key findings revealed: (i) Significantly lower Ct values for Group 1 versus Control 1 across bis293T/bisHT29 ($p<0.01$; Fig. 4A,B; Table 10); (ii) Comparable amplification efficiency between Group 2 and Controls 2-1/2-2 (Fig. 4C,D; Table 10); (iii) Superior performance of Group 3 versus Control 3, evidenced by reduced Ct ($p<0.01$), improved sigmoidal kinetics, and enhanced signal-to-background ratios (Fig. 4E,F; Table 10); (iv) Significantly decreased Ct for bisProAB1-optimized Group 4-1 versus Control 4 ($p<0.01$), whereas Groups 4-2/4-3 showed non-significant differences (Fig. 4G,H; Table 10). Critically, bisACTB_103_F2+R2+P2 and bisProAB1_F2+R2+P1 demonstrated the most substantial amplification efficiency gains, while bisACTB_89_F+R+P exhibited optimal reaction kinetics. Collectively, these three systems demonstrate robust applicability for DNA methylation quantification in diverse human cell models—spanning normal epithelia (293T) to carcinomas (HT29)—validating their utility as high-performance internal references.

Clinical Validation in Ovarian Tissues Affirms Enhanced Efficiency and Optimal Kinetics of Optimized Reference Systems

Building on this comparative framework, we next evaluated all primer-probe groups using bisDNA from ovarian carcinoma tissues (bisTOV) and adjacent normal tissues (bisAOV). Consistent with cell line observations: (i) Optimized Group 1 (bisACTB_103_F2+R2+P2) demonstrated significantly lower Ct values versus Control Group 1 for both bisTOV and bisAOV ($p<0.01$; Fig. 5A,B; Table 11); (ii) Group 2 (bisACTB_89_F+R+P) maintained comparable efficiency to Controls 2-1/2-2 (Fig. 5C,D; Table 11); (iii) Group 3 exhibited superior performance over Control 3, with reduced Ct ($p<0.01$), enhanced sigmoidal kinetics, and higher signal-to-background ratios (Fig. 5E,F; Table 11); (iv) bisProAB1-optimized Group 4-1 showed significantly decreased Ct versus Control 4 ($p<0.01$), while Groups 4-2/4-3 displayed non-significant differences (Fig. 5G,H; Table 11). Notably, bisACTB_103_F2+R2+P2 and bisProAB1_F2+R2+P1 again exhibited the most substantial amplification

efficiency gains, whereas bisACTB_89_F+R+P maintained optimal reaction kinetics. These collective findings demonstrate robust cross-tissue applicability of these three reference systems for DNA methylation quantification in both malignant (OVCA) and normal ovarian tissue specimens.

Clinically Validated ACTB Reference Systems Enable Ultrasensitive Plasma Methylation Detection

Blood represents a primary clinical biospecimen for cancer biomarker detection, with plasma/serum emerging as pivotal substrates for DNA methylation-based screening.

We validated primer-probe performance using bisDNA from blood cell pellets of benign disease (bisBBD) and ovarian cancer patients (bisBOV). Comprehensive TaqMan qPCR analysis revealed: (i) bisACTB_103_F2+R2+P2 achieved significantly lower Ct values versus Control 1 across all cohorts ($p<0.01$; Fig. 6A-C; Table 12); (ii) bisACTB_89_F+R+P maintained amplification efficiency comparable to Controls 2-1/2-2 (Fig. 6D-F; Table 12); (iii) Group 3 exhibited equivalent Ct values but superior sigmoidal kinetics and enhanced signal-to-noise ratios versus Control 3 (Fig. 6G-I; Table 12); (iv) bisProAB1_F2+R2+P1 demonstrated significantly reduced Ct versus Control 4 ($p<0.01$), while Groups 4-2/4-3 showed non-significant differences (Fig. 6J-L; Table 12). Critically, bisACTB_103_F2+R2+P2 and bisProAB1_F2+R2+P1 delivered the strongest amplification efficiency, whereas bisACTB_89_F+R+P generated optimal reaction kinetics in human blood cell specimens—collectively affirming their utility for hematological DNA methylation analysis.

Plasma-derived cell-free DNA (cfDNA) provides a critical reservoir for tumor DNA methylation biomarker discovery, yet its ultra-low concentration precludes accurate bisDNA quantification by conventional methods like NanoDrop™. Consequently, establishing sensitive internal reference standards is essential for determining bisDNA content and improving sample qualification rates. We therefore evaluated optimized primer-probe sets using bisulfite-converted plasma DNA from bisPBD and ovarian cancer patients (bisPOV). Key findings demonstrated: (i) bisACTB_103_F2+R2+P2 yielded significantly lower Ct values versus Control 1 across all plasma cohorts ($p<0.01$; Fig. 7A-C; Table 13); (ii) bisACTB_89_F+R+P maintained

comparable efficiency to Controls 2-1/2-2 (Fig. 7D-F; Table 13); (iii) Group 3 showed significantly reduced Ct for bisPBD ($p<0.01$) plus enhanced kinetics/signal-to-noise universally versus Control 3 (Fig. 7G-I; Table 13); (iv) bisProAB1_F2+R2+P1 exhibited markedly lower Ct versus Control 4 ($p<0.01$), while Groups 4-2/4-3 showed non-significant differences (Fig. 7J-L; Table 13). Critically, bisACTB_103_F2+R2+P2 and bisProAB1_F2+R2+P1 delivered superior amplification efficiency—particularly pivotal for low-abundance plasma cfDNA, enabling ≈2.8-fold lower detection limits (ΔCt≈1.5; Fig. 7L; Table 13). Collectively, these optimized systems significantly enhance detection sensitivity across diverse biospecimens (cell lines, tissues, blood cells, plasma), with transformative implications for improving sample qualification rates in plasma-based methylation biomarker studies.

DISCUSSION

Performance Comparison of Internal Reference Primers/Probes Using Single-Variable Design in Clinically Relevant Contexts

This study utilized gDNA) and bisDNA as reference templates—rather than synthetic gACTB/bisACTB plasmid constructs—for two critical reasons: First, synthetic templates only permit amplification efficiency assessment without evaluating specificity interference, whereas biological templates enable simultaneous evaluation of target amplification capacity and non-specificity exclusion. Second, different primer sets amplify distinct reference fragments; employing artificially synthesized internal controls would introduce multiple variables, precluding direct performance comparisons between primer sets. To implement this approach, we initially utilized gDNA and bisDNA from cervical carcinoma HeLa cells as unified templates for screening primer/probe sets via SYBR Green I and TaqMan qPCR. Optimized configurations were subsequently validated across diverse biospecimens—including bis293T/HT29 cell lines, gender-stratified tumor/adjacent tissues, blood cells, and plasma—ultimately identifying the highest-performance primer-probe combinations.

In practical tumor DNA methylation qPCR kit applications, positive/negative controls and test subjects comprise authentic biospecimens: bisDNA derived from cell lines, tumor/adjacent tissues, blood cells, and plasma samples. Our

study encompassed all these clinically relevant sample types. By optimizing reference primer-probe sets to enhance bisDNA amplification sensitivity and gDNA specificity, we improved detection qualification rates for low-concentration clinical specimens (particularly plasma) in probe-based qPCR assays. This optimization reduces precious sample wastage while potentially increasing kit detection positivity rates.

Primer design for bisDNA should prioritize stringent exclusion of gDNA amplification

Following bisulfite conversion, complementary strands of human gDNA lose sequence reciprocity. Consequently, primers designed against either converted strand must prioritize mitigation of gDNA interference. Systematic NCBI Primer-BLAST analysis of literature-derived, optimized, and novel primer sets revealed that only the bisACTB_103 primers from Zhang et al. [26], Wang et al.[27], and Bian et al.[28,29] exhibited perfect genomic matches to a 103-bp endogenous target. Dye-based qPCR validation confirmed significant gDNA amplification for this set, characterized by distinct melting peaks (85~90□; Supplementary Fig. 1A,D) and significantly lower Ct values versus bisDNA (Supplementary Table 1). Probe-based qPCR further demonstrated non-specific amplification with gDNA templates (Fig. 1B). Critically, given ubiquitous gDNA contamination in qMSP laboratories, such primer sets risk generating false-positive signals in negative controls—thereby compromising bisulfite conversion efficiency validation. In contrast, novel primer sets experimentally demonstrated undetectable gDNA amplification, confirming effective mitigation of genomic interference.

CpG-Free gACTB Fragments Eliminate Sequence Ambiguity from Site-Specific Methylation

The gACTB fragments referenced in prior studies[26] contain 1-2 CpG sites (Supplementary Sequence Information). While authors assumed these CpG sites remain unmethylated (designing bisACTB primers against T templates), emerging evidence indicates *ACTB* methylation occurs in pathologies like stroke[37] and coronary heart disease[38]. In such cases, methylated cytosines resist conversion, creating sequence heterogeneity at CpG sites. Primers targeting unconverted T templates may fail to amplify these variants,

compromising internal reference functionality and sample qualification rates. To address this, we selected two CpG-free gACTB fragments and one CpG-free *ACTB* promoter fragment (bisAB1/bisAB2/bisProAB1) as reference regions, ensuring conversion consistency. Future studies should screen additional CpG-free genomic regions to develop higher-performance reference systems.

MGB Probes Overcome Primer-Dimer Interference to Restore BisACTB qPCR Efficiency

In SYBR Green assays, control primers for bisACTB_89 (FP+RP-1/FP+RP-2) and bisACTB_78 (F2+R2) showed significantly higher Ct values versus optimized sets (Supplementary Fig. 2D-F; Supplementary Tables 3,5). Strikingly, probe-based qPCR revealed equivalent efficiency between control and optimized combinations when paired with MGB probes (Fig. 1D,G; Supplementary Tables 4,6). This suggests primer-dimers suppressed target amplification in dye-based assays, while MGB probes likely counteracted such interference—potentially through enhanced specificity—to restore amplification efficiency.

High-Efficiency Reference Systems Establish Performance Benchmarks for DNA Methylation Biomarker Assays

Through multi-parameter optimization—including Tm harmonization (58-62□), dimer-disrupting mutations, NCBI Primer-BLAST verification, and probe positioning adjustments—we developed reference sets achieving ΔCt = -1.5 versus controls (Fig. 7L; Table 13). Since each ΔCt = -1 reflects 2-fold sensitivity gain, these high-efficiency references not only improve sample qualification rates but also establish performance benchmarks for biomarker assays. We propose a ΔCt-based quality metric: Biomarker primers performing within ±0.5 ΔCt of the reference are "qualified"; >+0.5 ΔCt indicates "substandard"; <-0.5 ΔCt denotes "excellent". Implementing such standardized evaluation frameworks will accelerate translational development of DNA methylation biomarkers across research, diagnostic, and clinical domains.

Figure legends of Supplementary Figures

Supplementary Figure 1: SYBR green qPCR assays. (A–C) (A) bisACTB_103_F1 + bisACTB_103_R1, (B) bisACTB_103_F2 + bisACTB_103_R2, and (C) bisACTB_103_F2_17C + bisACTB_103_R2 primer combinations for the melting curves of bisHela, gHela, and BC. (D–F) (D) bisACTB_103_F1 + bisACTB_103_R1, (E) bisACTB_103_F2 + bisACTB_103_R2, and (F) bisACTB_103_F2_17C + bisACTB_103_R2 primer combinations for the original curves of bisHela (solid line with triangle), gHela（solid line with square）, and BC（solid line with circle）.

Supplementary Figure 2: SYBR green qPCR assays. (A–C) (A) bisACTB_89_FP + bisACTB_89_RP-1, (B) bisACTB_89_FP + bisACTB_89_RP-2, and (C) bisACTB_89_F + bisACTB_89_R primer combinations for the melting curves of bisHela, gHela, and BC. (D–F) (D) bisACTB_89_FP + bisACTB_89_RP-1, (E) bisACTB_89_FP + bisACTB_89_RP-2, and (F) bisACTB_89_F + bisACTB_89_R primer combinations for the original curves of bisHela (solid line with triangle), gHela（solid line with square）, and BC（solid line with circle）.

Supplementary Figure 3: SYBR green qPCR assays. (A–C) (A) bisACTB_78_F2 + bisACTB_78_R2, (B) bisACTB_78_F23 + bisACTB_89_R, and (C) bisACTB_78_F3_19C + bisACTB_89_R primer combinations for the melting curves of bisHela, gHela, and BC. (D–F) (D) bisACTB_78_F2 + bisACTB_78_R2, (E) bisACTB_78_F23 + bisACTB_78_R, and (F) bisACTB_78_F3_19C + bisACTB_89_R primer combinations for the original curves of bisHela (solid line with triangle), gHela（solid line with square）, and BC（solid line with circle）.

Supplementary Figure 4: SYBR green qPCR assays. (A–C) bisProAB1_F + bisProAB1_R (dashed line with circle), bisProAB1_F1 + bisProAB1_R1（solid line with square）, and bisProAB1_F2 + bisProAB1_R2（solid line with triangle） primer combinations for (A) bisHela, (B) gHela, and (C) BC melting curves. (D–F) bisProAB1_F + bisProAB1_R, bisProAB1_F1 + bisProAB1_R1, and bisProAB1_F2 + bisProAB1_R2 primer combinations for (D) bisHela, (E) gHela, and (F) BC original curves.

Figure legends of Figures

Figure 1: Amplification profiles from TaqMan probe-based qPCR assays. (A~C) Amplification curves of bisACTB_103 primer-probe sets for (A) bisHeLa, (B) gHeLa, and (C) blank control (BC). (D~F) Amplification curves of bisACTB_89 primer-probe sets for (D) bisHeLa, (E) gHeLa, and (F) BC. (G~I) Amplification curves of bisACTB_78 primer-probe sets for (G) bisHeLa, (H) gHeLa, and (I) BC.

Figure 2: Amplification profiles from TaqMan probe-based qPCR assays. (A-C) Amplification

curves generated by the bisAB1_F4/R4/P4 primer-probe set for (A) bisHeLa (B) gHeLa, and (C) blank control (BC). (D-F) Amplification curves produced by the bisAB1_F4/R4-2/P4 combination for (D) bisHeLa, (E) gHeLa, and (F) BC. (G-I) Amplification profiles obtained with the bisAB1_F4-2/R4/P4 set for (G) bisHeLa, (H) gHeLa, and (I) BC. (J-L) Amplification curves using the bisAB2_F4/R4/P4 system for (J) bisHeLa, (K) gHeLa, and (L) BC.

Figure 3: Amplification profiles of bisProAB1 primer-probe sets in TaqMan qPCR assays. (A-C) Amplification curves for (A) bisHeLa, (B) gHeLa, and (C) blank control (BC).

Figure 4: Amplification profiles from probe-based qPCR assays. (A-B) Amplification curves of bisACTB_103 primer-probe sets for (A) bis293T and (B) bisHT29, comparing control and experimental groups. (C-D) Amplification curves of bisACTB_89 primer-probe sets for (C) bis293T and (D) bisHT29 (control vs. experimental groups). (E-F) Amplification curves of bisACTB_78 primer-probe sets for (E) bis293T and (F) bisHT29 (control vs. experimental groups). (G-H) Amplification profiles of bisProAB1, bisAB1, and bisAB2 primer-probe sets for (G) bis293T and (H) bisHT29 (control vs. experimental groups).

Figure 5: Amplification profiles from TaqMan probe-based qPCR assays. (A-B) Amplification curves of bisACTB_103 primer-probe sets in (A) bisTOV and (B) bisAOV, comparing control and experimental groups. (C-D) Amplification curves of bisACTB_89 primer-probe sets in (C) bisTOV and (D) bisAOV (control vs. experimental). (E-F) Amplification curves of bisACTB_78 primer-probe sets in (E) bisTOV and (F) bisAOV (control vs. experimental). (G-H) Amplification profiles of bisProAB1/bisAB1/bisAB2 primer-probe combinations in (G) bisTOV and (H) bisAOV (control vs. experimental).

Figure 6: Amplification profiles from TaqMan probe-based qPCR assays. (A, B) Amplification curves of bisACTB_103 primer-probe sets in (A) bisBBD, (B) bisBOV, comparing control and experimental groups. (C, D) Amplification curves of bisACTB_89 primer-probe sets in (C) bisBBD, (D) bisBOV (control vs. experimental). (E, F) Amplification curves of bisACTB_78 primer-probe sets in (E) bisBBD, (F) bisBOV (control vs. experimental). (G, H) Amplification profiles of bisProAB1/bisAB1/bisAB2 primer-probe combinations in (G) bisBBD, (H) bisBOV (control vs. experimental).

Figure 7: Amplification profiles from TaqMan probe-based qPCR assays. (A, B) Amplification curves of bisACTB_103 primer-probe sets in (A) bisPBD, (B) bisPOV, comparing control and experimental groups. (C, D) Amplification curves of bisACTB_89 primer-probe sets in (C) bisPBD, (D) bisPOV (control vs. experimental). (E, F) Amplification curves of bisACTB_78 primer-probe sets in (E) bisPBD, (F) bisPOV (control vs. experimental). (G, H) Amplification profiles of bisProAB1/bisAB1/bisAB2 primer-probe combinations in (G) bisPBD, (H) bisPOV

(control vs. experimental).

AUTHOR CONTRIBUTIONS

Shan Zhang: Collected and collated various types of samples and associated clinical information; organized experimental data and performed statistical analysis; revised the manuscript. Jiahui Jiang: Conducted all experimental work; organized experimental results and performed preliminary analysis; revised the manuscript. Ling Chen: Designed the experimental protocols; analyzed experimental results and performed figure preparation; wrote, developed, and finalized the manuscript.

ACKNOWLEDGMENTS

The authors greatly thank Xianyou Yi for her support. The authors would like to thank Yisheng Li, and Rong Wu for their valuable help.

CONFLICT OF INTEREST STATEMENT

The authors have no conflict of interest.

DATA AVAILABILITY STATEMENT

All raw data and code are available upon request.

FUNDING INFORMATION

This study was supported by the Hunan Provincial Natural Science Foundation Joint Fund for the Healthcare Industry (Grant No. 2025JJ81155)

ETHICS STATEMENT

Written informed consent was obtained from all individuals whose residual samples were used in this study. These residual samples comply with relevant ethical guidelines, including the Declaration of Helsinki, and the study received formal approval from the Clinical Research Management Committee of Zhangjiajie People's Hospital (Approval No: LL-2025-0017).

REFERENCES

1. Tumor marker committee of Chinese anti-cancer association. Expert consensus on detection and clinical application of tumor DNA methylation biomarkers (2024 edition) [J]. Chin J Cancer Prev Treat, 2024, 16(2): 129-142.

2. Ibrahim, J., Peeters, M., Van Camp, G. & Op de Beeck, K. Methylation biomarkers for early cancer detection and diagnosis: Current and future perspectives. *European Journal of Cancer* **178**, 91-113 (2023).
3. Yang, Y., Wen, X. & Wang, L. Advancements in DNA methylation technologies and their application in cancer diagnosis. *Epigenetics* **20**, 2539995 (2025).
4. Sigalotti, L., Covre, A., Colizzi, F. & Fratta, E. Quantitative Methylation-Specific PCR: A Simple Method for Studying Epigenetic Modifications of Cell-Free DNA. in *Cell-free DNA as Diagnostic Markers: Methods and Protocols* (eds. Casadio, V. & Salvi, S.) 137-162 (Springer New York, New York, NY, 2019).
5. Wu, Y.*, et al.* A novel dual-target Septin9 methylation assay for improved detection of early-stage colorectal cancer and high-grade intraepithelial neoplasia. *BMC cancer* **24**, 916 (2024).
6. Zhu, D.*, et al.* Highly specific multiplex DNA methylation detection for liquid biopsy of colorectal cancer. *Clinica Chimica Acta* **565**, 120026 (2025).
7. Demokan, S.*, et al.* KIF1A and EDNRB are differentially methylated in primary HNSCC and salivary rinses. *International journal of cancer* **127**, 2351-2359 (2010).
8. Hong, Y. & Kim, W.J. DNA Methylation Markers in Lung Cancer. *Current genomics* **22**, 79-87 (2021).
9. Guo, D.Z.*, et al.* Early detection and prognosis evaluation for hepatocellular carcinoma by circulating tumour DNA methylation: A multicentre cohort study. *Clinical and translational medicine* **14**, e1652 (2024).
10. Fu, S.*, et al.* Genome-Wide Methylation Sequencing to Identify DNA Methylation Markers for Early-stage Hepatocellular Carcinoma in Liver and Blood. *Journal of Experimental & Clinical Cancer Research* **44**, 144 (2025).
11. Hum, M. & Lee, A.S.G. DNA methylation in breast cancer: early detection and biomarker discovery through current and emerging approaches. *Journal of Translational Medicine* **23**, 465 (2025).
12. Tao, M.*, et al.* Multiplex methylation detection assays using a blocking FRET probe with machine learning-assisted quantitative melting curve method targeting early-stage breast cancer. *Chemical Engineering Journal* **498**, 155093 (2024).
13. Torng, P.L.*, et al.* Promoter methylation of IGFBP-3 and p53 expression in ovarian endometrioid carcinoma. *Molecular cancer* **8**, 120 (2009).
14. Reesink-Peters, N.*, et al.* Detecting cervical cancer by quantitative promoter hypermethylation assay on cervical scrapings: a feasibility study. *Molecular cancer research : MCR* **2**, 289-295 (2004).
15. Hayashi, M.*, et al.* Epigenetic inactivation of VGF associated with Urothelial Cell Carcinoma and its potential as a non-invasive biomarker using urine. *Oncotarget* **5**, 3350-3361 (2014).
16. Maldonado, L.*, et al.* An epigenetic marker panel for recurrence risk prediction of low grade papillary urothelial cell carcinoma (LGPUCC) and its potential use for surveillance after transurethral resection using urine. *Oncotarget* **5**, 5218-5233 (2014).
17. Oh, T.J.*, et al.* Feasibility of quantifying SDC2 methylation in stool DNA

for early detection of colorectal cancer. *Clinical epigenetics* **9**, 126 (2017).
18. Carvalho, A.L., *et al.* Detection of promoter hypermethylation in salivary rinses as a biomarker for head and neck squamous cell carcinoma surveillance. *Clinical cancer research : an official journal of the American Association for Cancer Research* **17**, 4782-4789 (2011).
19. Park, S.J., *et al.* Combination Analysis of PCDHGA12 and CDO1 DNA Methylation in Bronchial Washing Fluid for Lung Cancer Diagnosis. *Journal of Korean medical science* **39**, e28 (2024).
20. Dillinger, T., *et al.* Identification of tumor tissue-derived DNA methylation biomarkers for the detection and therapy response evaluation of metastatic castration resistant prostate cancer in liquid biopsies. *Molecular cancer* **21**, 7 (2022).
21. Yuan, T., *et al.* Methylation-based smoking signatures in blood and tissue samples for the prediction of self-reported smoking status and mortality in patients with colorectal cancer. *Clinical epigenetics* **17**, 113 (2025).
22. Grützmann, R., *et al.* Sensitive detection of colorectal cancer in peripheral blood by septin 9 DNA methylation assay. *PloS one* **3**, e3759 (2008).
23. Oh, T., *et al.* Genome-wide identification and validation of a novel methylation biomarker, SDC2, for blood-based detection of colorectal cancer. *The Journal of molecular diagnostics : JMD* **15**, 498-507 (2013).
24. Tan, S.H., *et al.* Detection of promoter hypermethylation in serum samples of cancer patients by methylation-specific polymerase chain reaction for tumour suppressor genes including RUNX3. *Oncology reports* **18**, 1225-1230 (2007).
25. Miller, B.F., Petrykowska, H.M. & Elnitski, L. Assessing ZNF154 methylation in patient plasma as a multicancer marker in liquid biopsies from colon, liver, ovarian and pancreatic cancer patients. *Sci Rep* **11**, 221 (2021).
26. Zhang, L., *et al.* Methylation of SDC2/TFPI2 and Its Diagnostic Value in Colorectal Tumorous Lesions. *Frontiers in molecular biosciences* **8**, 706754 (2021).
27. Wang, Z., *et al.* Evaluating the Clinical Performance of a Dual-Target Stool DNA Test for Colorectal Cancer Detection. *The Journal of Molecular Diagnostics* **24**, 131-143 (2022).
28. Bian, Y., *et al.* Genome-wide methylation profiling identified methylated KCNA3 and OTOP2 as promising diagnostic markers for esophageal squamous cell carcinoma. *Chinese Medical Journal*, 10.1097/CM1099.0000000000002832 (2023).
29. Bian, Y., *et al.* Non-invasive diagnosis of esophageal cancer by a simplified circulating cell-free DNA methylation assay targeting OTOP2 and KCNA3: a double-blinded, multicenter, prospective study. *Journal of Hematology & Oncology* **17**, 47 (2024).
30. Li, R., *et al.* Identification of two methylated fragments of an SDC2 CpG island using a sliding window technique for early detection of colorectal cancer. *FEBS open bio* **11**, 1941-1952 (2021).
31. Zhao, Y., *et al.* Plasma methylated GNB4 and Riplet as a novel dual-marker panel for the detection of hepatocellular carcinoma. *Epigenetics* **19**, 2299044 (2024).
32. Wang, L., *et al.* Hypermethylated CDO1 and ZNF454 in Cytological

Specimens as Screening Biomarkers for Endometrial Cancer. *Frontiers in oncology* **12**, 714663 (2022).

33. Kutyavin, I.V.*, et al.* 3′-Minor groove binder-DNA probes increase sequence specificity at PCR extension temperatures. *Nucleic Acids Research* **28**, 655-661 (2000).
34. Zeschnigk, M.*, et al.* A novel real-time PCR assay for quantitative analysis of methylated alleles (QAMA): analysis of the retinoblastoma locus. *Nucleic Acids Res* **32**, e125 (2004).
35. Yao, Y., Nellåker, C. & Karlsson, H. Evaluation of minor groove binding probe and Taqman probe PCR assays: Influence of mismatches and template complexity on quantification. *Molecular and Cellular Probes* **20**, 311-316 (2006).
36. Yangyang Liu, Hengmi Cui. The method of estimating bisulfite conversion rate in DNA methylation analysis[J]. HEREDITAS(Beijing), 2015, 37(9): 939-944.
37. Liu, C.*, et al.* ACTB Methylation in Blood as a Potential Marker for the Pre-clinical Detection of Stroke: A Prospective Nested Case-Control Study. *Frontiers in neuroscience* **15**, 644943 (2021).
38. Jin, J., Zhu, C., Wang, J., Zhao, X. & Yang, R. The association between ACTB methylation in peripheral blood and coronary heart disease in a case-control study. *Frontiers in cardiovascular medicine* **9**, 972566 (2022).

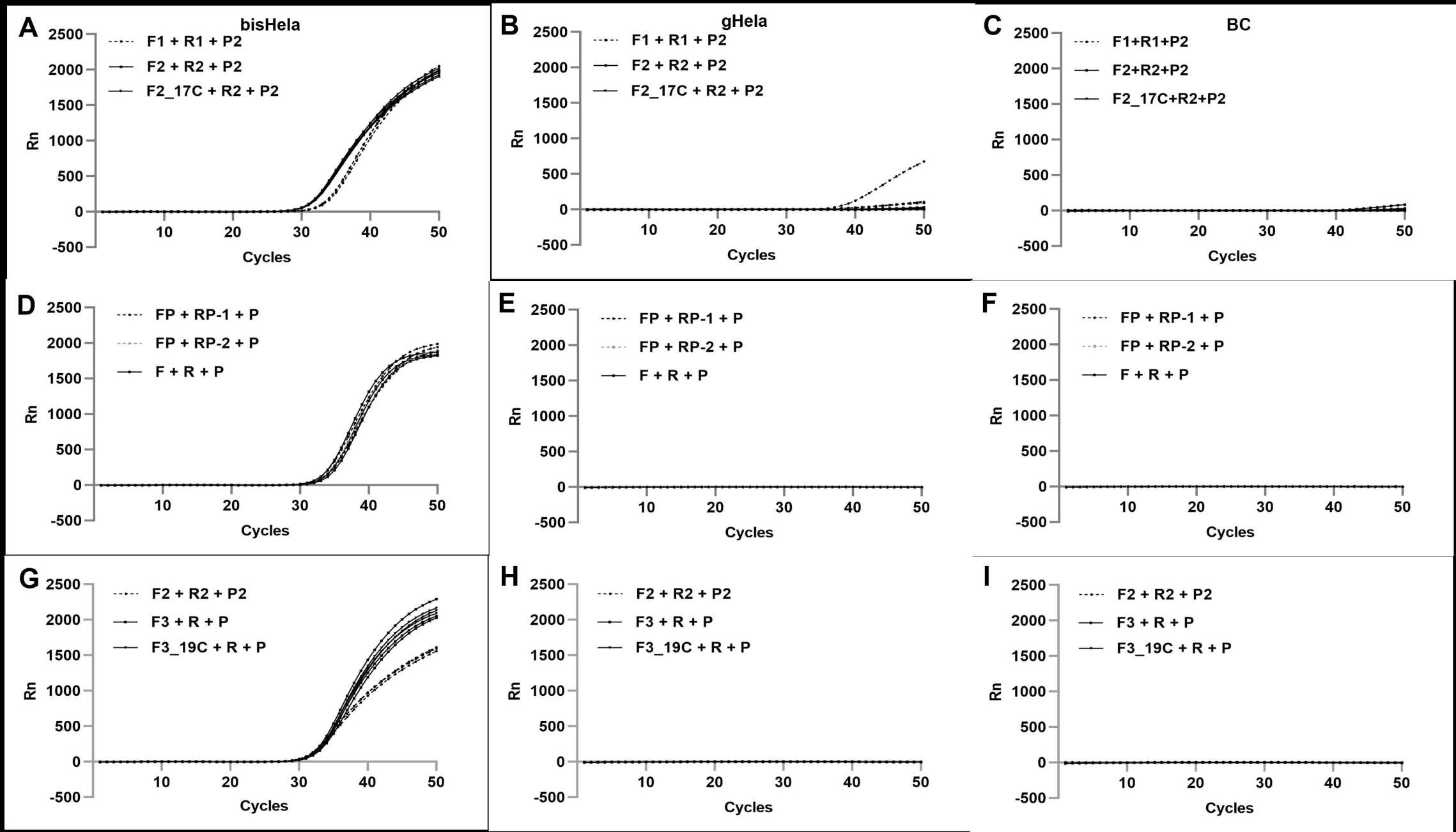
A
bisHela
F1 + R1 + P2
F2 + R2 + P2
F2_17C + R2 + P2
B
gHela
F1 + R1 + P2
F2 + R2 + P2
F2_17C + R2 + P2
C
BC
F1+R1+P2
F2+R2+P2
F2_17C+R2+P2
D
FP + RP-1 + P
FP + RP-2 + P
F + R + P
E
FP + RP-1 + P
FP + RP-2 + P
F + R + P
F
FP + RP-1 + P
FP + RP-2 + P
F + R + P
G
F2 + R2 + P2
F3 + R + P
F3_19C + R + P
H
F2 + R2 + P2
F3 + R + P
F3_19C + R + P
I
F2 + R2 + P2
F3 + R + P
F3_19C + R + P
Rn
Cycles
2500
2000
1500
1000
500
0
-500
10
20
30
40
50

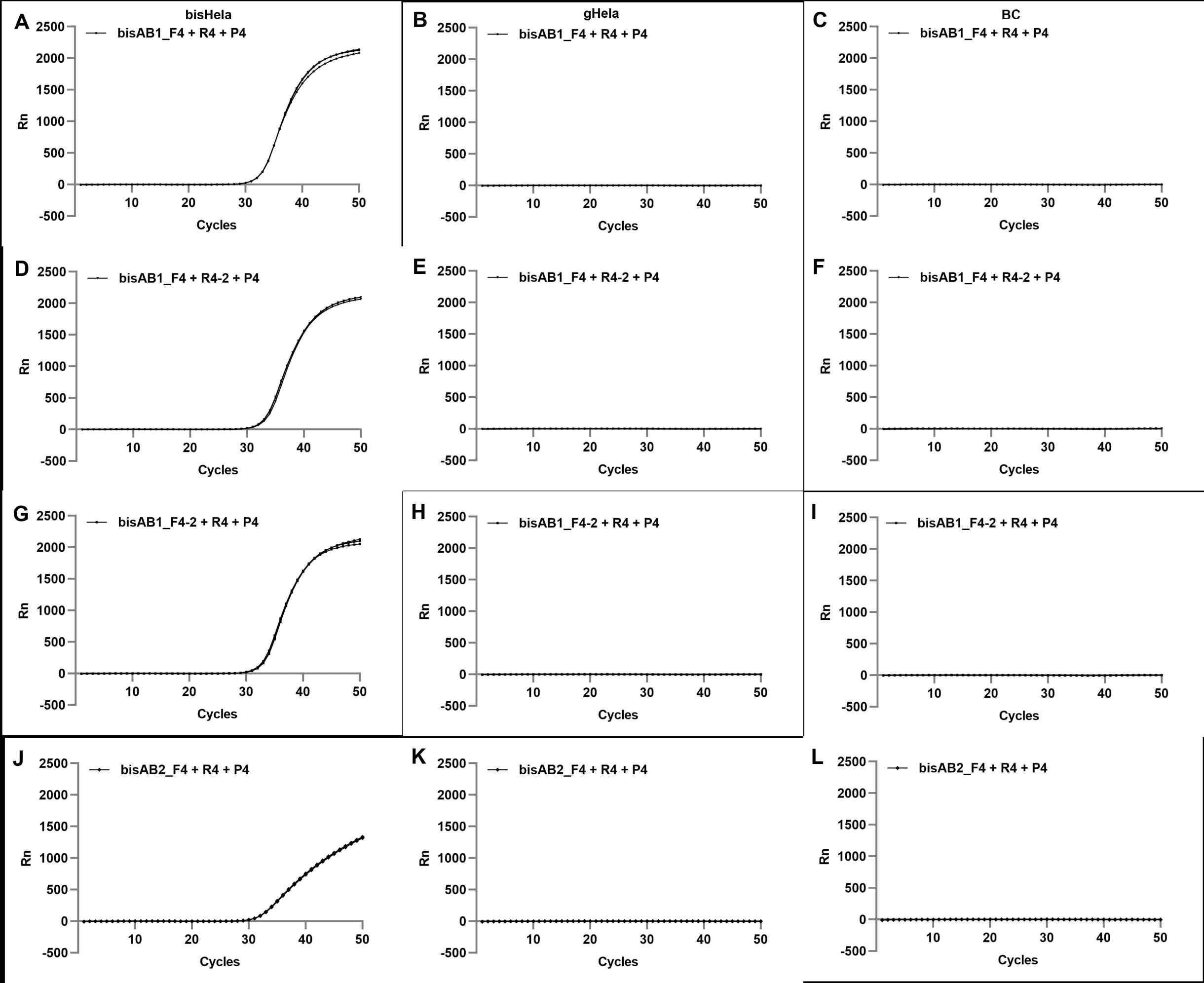
A
bisHela
bisAB1_F4 + R4 + P4
B
gHela
bisAB1_F4 + R4 + P4
C
BC
bisAB1_F4 + R4 + P4
D
bisAB1_F4 + R4-2 + P4
E
bisAB1_F4 + R4-2 + P4
F
bisAB1_F4 + R4-2 + P4
G
bisAB1_F4-2 + R4 + P4
H
bisAB1_F4-2 + R4 + P4
I
bisAB1_F4-2 + R4 + P4
J
bisAB2_F4 + R4 + P4
K
bisAB2_F4 + R4 + P4
L
bisAB2_F4 + R4 + P4
Rn
Cycles
2500
2000
1500
1000
500
0
-500
10
20
30
40
50

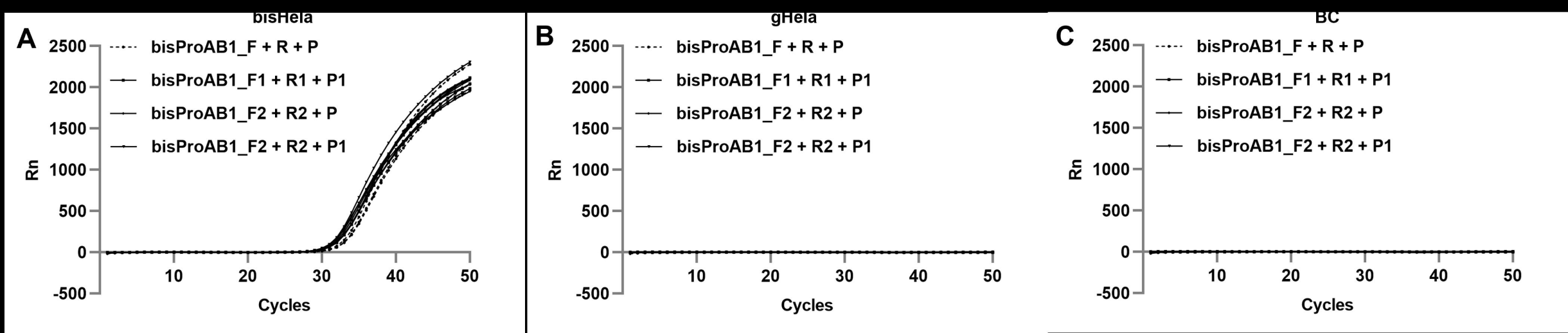
A
bisHela
bisProAB1_F + R + P
bisProAB1_F1 + R1 + P1
bisProAB1_F2 + R2 + P
bisProAB1_F2 + R2 + P1
Rn
Cycles
B
gHela
bisProAB1_F + R + P
bisProAB1_F1 + R1 + P1
bisProAB1_F2 + R2 + P
bisProAB1_F2 + R2 + P1
Rn
Cycles
C
BC
bisProAB1_F + R + P
bisProAB1_F1 + R1 + P1
bisProAB1_F2 + R2 + P
bisProAB1_F2 + R2 + P1
Rn
Cycles

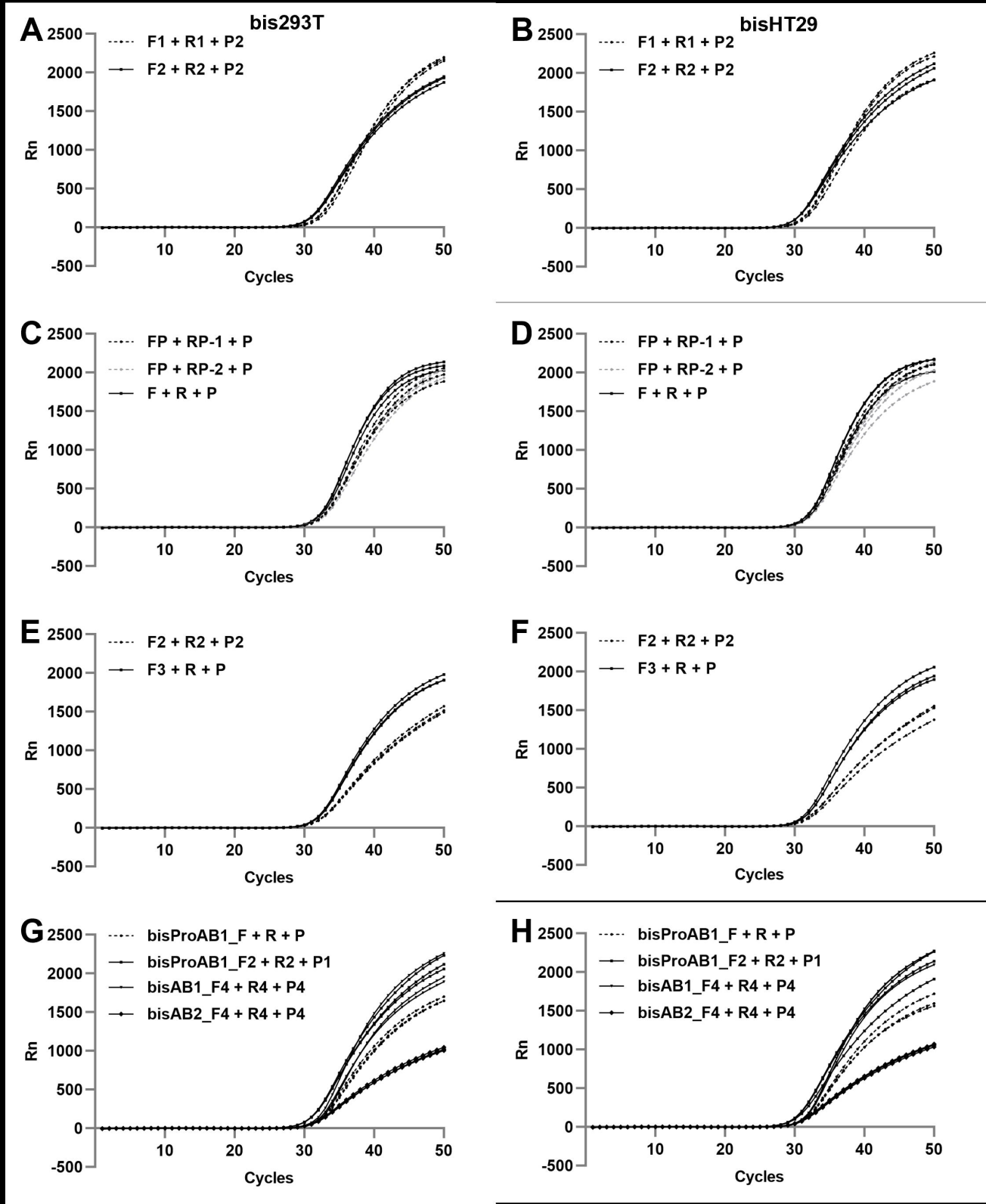
A
bis293T
F1 + R1 + P2
F2 + R2 + P2
B
bisHT29
F1 + R1 + P2
F2 + R2 + P2
C
FP + RP-1 + P
FP + RP-2 + P
F + R + P
D
FP + RP-1 + P
FP + RP-2 + P
F + R + P
E
F2 + R2 + P2
F3 + R + P
F
F2 + R2 + P2
F3 + R + P
G
bisProAB1_F + R + P
bisProAB1_F2 + R2 + P1
bisAB1_F4 + R4 + P4
bisAB2_F4 + R4 + P4
H
bisProAB1_F + R + P
bisProAB1_F2 + R2 + P1
bisAB1_F4 + R4 + P4
bisAB2_F4 + R4 + P4
Rn
Cycles
2500
2000
1500
1000
500
0
-500
10
20
30
40
50

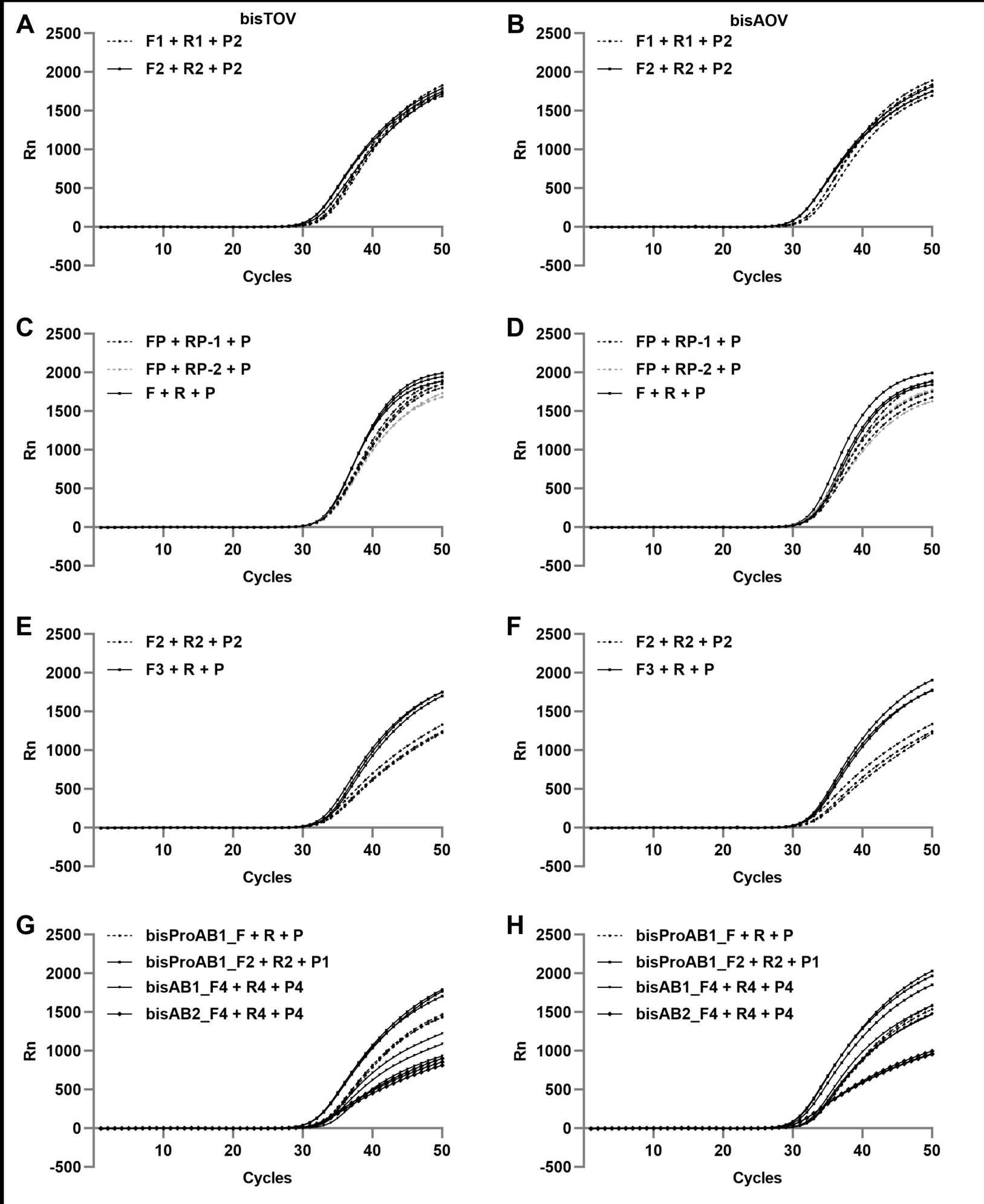
A
bisTOV
F1 + R1 + P2
F2 + R2 + P2
B
bisAOV
F1 + R1 + P2
F2 + R2 + P2
C
FP + RP-1 + P
FP + RP-2 + P
F + R + P
D
FP + RP-1 + P
FP + RP-2 + P
F + R + P
E
F2 + R2 + P2
F3 + R + P
F
F2 + R2 + P2
F3 + R + P
G
bisProAB1_F + R + P
bisProAB1_F2 + R2 + P1
bisAB1_F4 + R4 + P4
bisAB2_F4 + R4 + P4
H
bisProAB1_F + R + P
bisProAB1_F2 + R2 + P1
bisAB1_F4 + R4 + P4
bisAB2_F4 + R4 + P4
Rn
Cycles
2500
2000
1500
1000
500
0
-500
10
20
30
40
50

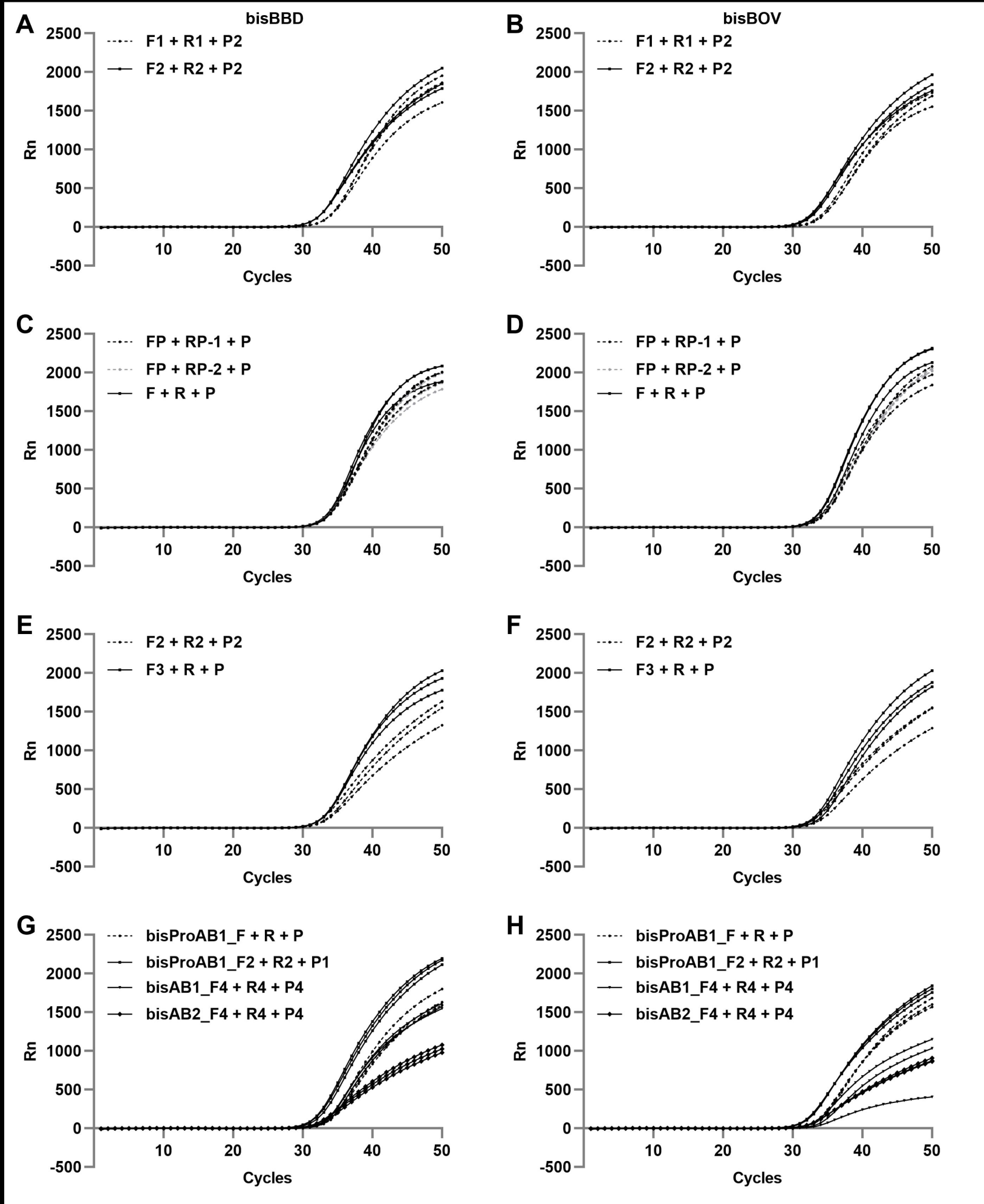
A
bisBBD
F1 + R1 + P2
F2 + R2 + P2
B
bisBOV
F1 + R1 + P2
F2 + R2 + P2
C
FP + RP-1 + P
FP + RP-2 + P
F + R + P
D
FP + RP-1 + P
FP + RP-2 + P
F + R + P
E
F2 + R2 + P2
F3 + R + P
F
F2 + R2 + P2
F3 + R + P
G
bisProAB1_F + R + P
bisProAB1_F2 + R2 + P1
bisAB1_F4 + R4 + P4
bisAB2_F4 + R4 + P4
H
bisProAB1_F + R + P
bisProAB1_F2 + R2 + P1
bisAB1_F4 + R4 + P4
bisAB2_F4 + R4 + P4
Rn
Cycles
2500
2000
1500
1000
500
0
-500
10
20
30
40
50

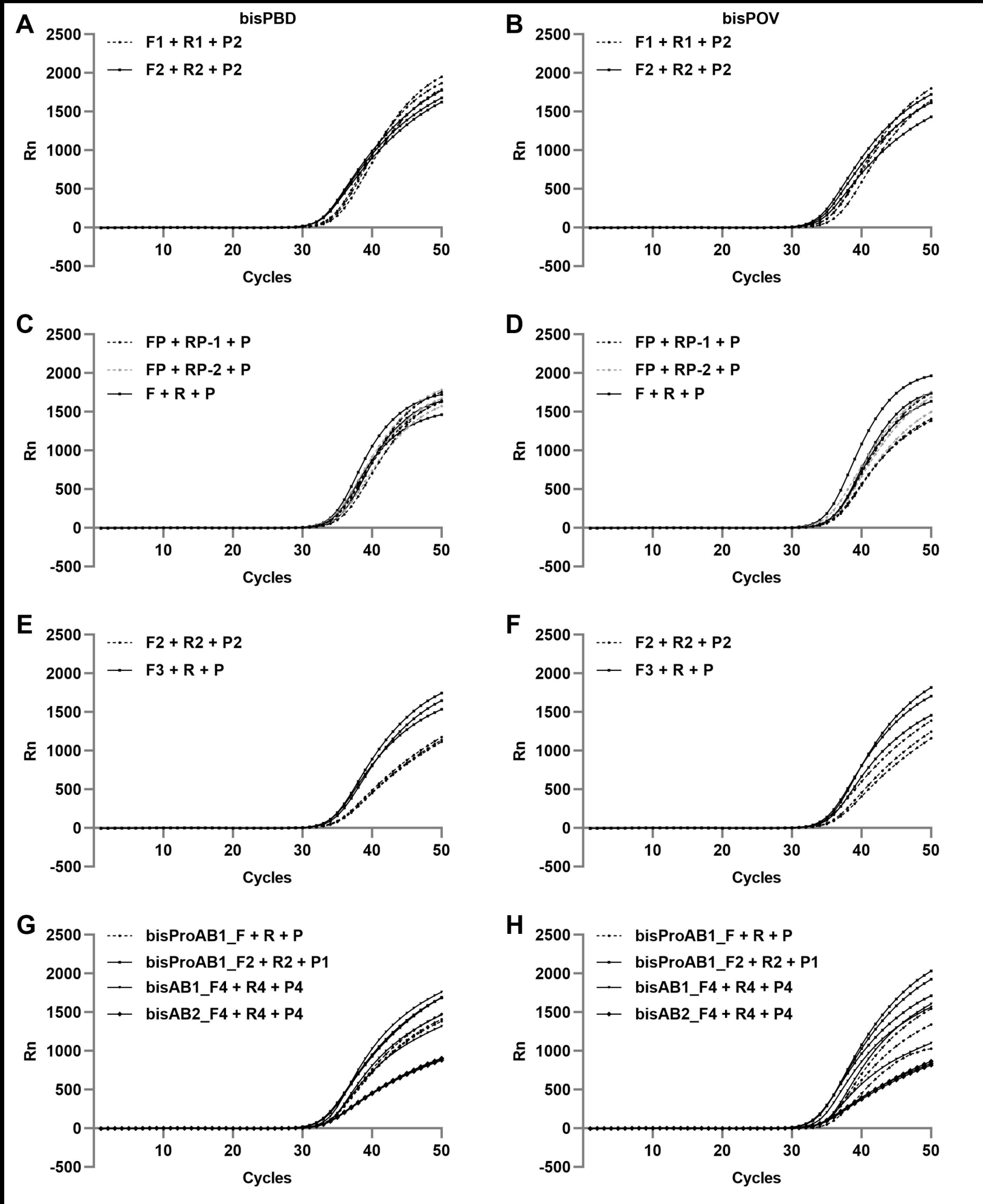
A
bisPBD
F1 + R1 + P2
F2 + R2 + P2
B
bisPOV
F1 + R1 + P2
F2 + R2 + P2
C
FP + RP-1 + P
FP + RP-2 + P
F + R + P
D
FP + RP-1 + P
FP + RP-2 + P
F + R + P
E
F2 + R2 + P2
F3 + R + P
F
F2 + R2 + P2
F3 + R + P
G
bisProAB1_F + R + P
bisProAB1_F2 + R2 + P1
bisAB1_F4 + R4 + P4
bisAB2_F4 + R4 + P4
H
bisProAB1_F + R + P
bisProAB1_F2 + R2 + P1
bisAB1_F4 + R4 + P4
bisAB2_F4 + R4 + P4
Rn
Cycles
2500
2000
1500
1000
500
0
-500
10
20
30
40
50